Proceedings of the Project Review, Geo-Mathematical Imaging Group (Purdue University, West Lafayette IN), Vol. 1 (2010) pp. 201-210.

THE EFFECT OF INITIAL CONTACT AREA ON THE MECHANICAL AND HYDRAULIC PROPERTIES OF SINGLE FRACTURES.

CHRISTOPHER PETROVITCH*, LAURA J. PYRAK-NOLTE†, AND DAVID D. NOLTE‡

Abstract. Experimental work suggests that the flow-stiffness relationship in single fractures relies on the geometry of the fracture, i.e. the size and spatial distributions of the void and contact area. In this work, the effect of the initial contact area on the deformation of fractures and fluid through fractures are analyzed. Fractures with both uncorrelated and correlated aperture distributions, with varying initial contact areas are deformed numerically under a normal load. When the displacement-stress and stiffness-stress curves are normalized by the initial contact area fraction, the disparate behavior collapses to a single curve except when the initial contact fraction approaches zero, for correlated fractures.To remove the dispersion for correlated fractures additional geometric length scales are needed to complete the normalization. The hydraulic properties normalization lends to bounding the possible flow-stiffness curves.

1. Introduction. In today's world, we rely upon the earth's subsurface in many ways. These include the extraction of drinkable water, production of oil and gas, nuclear waste disposal, the storage of anthropogenic byproducts (e.g. CO_2) in subsurface reservoirs, and the construction of subsurface structures, such as tunnels, underground buildings, and the foundations of dams and bridges. To successfully plan for any of these projects, an understanding of the geologic structures in the subsurface is required. This knowledge is very difficult to obtain because the earth's subsurface is composed of a hierarchy of processes that occur at scales that span many orders of magnitude. In this paper, we refer to a "fracture" with the understanding that we are referring to mechanical discontinuities that range in scale from lattice dislocations (10^{-9} m) to micro-cracks (10^{-6} m) to fractures (1 m) to the scale of plate boundaries (10^4 m).

To study processes with this range of scales, many scientists turn to the framework provided by Percolation Theory and more specifically finite-size scaling methods. Percolation Theory has been successfully used to predict many other physical processes that occur at different scales, such as, phase transitions, the spreading of forest fires, and the electrical conductance through random mediums [12]. However, in order to use these methods, a firm understanding of the properties of a physical system is required at each scale. For example, when considering 2D random site percolation, the common parameter used is the site occupation probability, p. To understand the system, the desired quantity is measured at various values of p and scale, L, to locate the critical probability, p_c, at the infinite limit via finite size scaling [12]. A goal is to apply these methods to the flow-stiffness relationship for single fractures by using the void/contact area fraction as our order parameter rather than the site occupation probability. Before this can be done, it must be recognized that in the previous example, each 2D pattern generated for a given probability is uniquely defined, e.g. depending on the value of p, a site is either occupied or not. This is not the case in the flow-stiffness relationship. For any given fracture, the void/contact area can be an effect of (1) its original configuration (similar to site percolation) and (2) the current load applied. In other words, it is a function of its initial state and how the fracture has been deformed under a load. In this study, we determined that the fracture displacement and stiffness as a function of stress, reduces to a single curve, through normalization by geometric parameters of the fracture. Also, the flow-stress curves are bounded by normalizing the flow by the initial void area fractions and mean aperture. Understanding the displacement-stress, stiffness-stress, and flow-stress behavior is the necessary first step in the study of the flow-stiffness relationship.

2. Fracture Model. In this study, the simulated fracture void geometries are generated using a stratified percolation method [9, 7, 8]. While many methods are based on bringing two generated rough surfaces together, (Pietgen & Saupe, [10]; Brown, [1]; Glover et al., [4]; Borodich &

*Department of Physics, Purdue University, West Lafayette, IN 47907

†Department of Physics, Purdue University, West Lafayette, IN 47907, Department of Earth and Atmospheric Sciences, Purdue University, West Lafayette, IN 47907

‡Department of Physics, Purdue University, West Lafayette, IN 47907

TABLE 2.1

Fracture generation parameters: (Left) Uncorrelated, (Right) Correlated. C_f is the approximate contact fraction to be expected. The aperture scaling is the parameter used to convert pixel overlap during the generation to a physical length. All fractures were generated with an edge length of 256 pixels and a physical dimension of .1 meters.

Uncorrelated	
NPTS (C_f)	Aperture Scaling (μm)
3800 (40%)	5.92105
4300 (35%)	5.23256
5000 (30%)	4.5000
5700 (25%)	3.94737
6600 (20%)	3.40909
7800 (15%)	2.88462
9700 (10%)	2.31959
12400 (5%)	1.81452

Correlated	
NPTS	Aperture Scaling (μm)
11	10.928
12	7.816049
13	5.602044
14	4.16493
15	3.160493
16	2.4414
17	1.915686
18	1.524158
19	1.22773
20	1.00000

Onishchenko, [1]; Walsh et al., [15]) , the stratified percolation method enables the user to control the void spaces directly, rather than indirectly. This method constructs a two-dimensional hierarchical aperture distribution with a tunable spatial correlation. The construction begins with a two-dimensional array set to zero. This initial array is termed the first tier. Within that tier, NPTS (number of points per tier) are selected and used to define the center of the next tier. This next tier is smaller than the first tier by a scale factor, b. This process is repeated until the desired number of tiers have been generated. Finally, within the final tiers, NPTS points of a given size are randomly placed and the initial array incremented by one unit. Overlapping tiers result in spatially-correlated aperture distributions.

Two types of fractures are considered in this study: (1) spatially uncorrelated (or random) and (2) spatially correlated. The uncorrelated patterns were generated by using only one tier, with NPTS points of a given size (4 pixels by 4 pixels) on a 2D array. The correlated patterns were generated using four tiers, with a scale factor set such that the final tier was the size of a plotted point (4 pixels by 4 pixels). In this paper, we only considred fractures of size 256 x 256 pixels, with a physical dimension of 0.1 meters on a side. Table 2.1 lists all of the parameter sets used to generate the fracture geometries for this study and an example of each set is shown in Figure 1.

3. Deformation Model. Understanding how a fracture deforms when subject to a load is necessary when investigating the relationship between the mechanical and hydraulic properties of fractures. In this study, fractures were deformed numerically under a normal load using a method similar to that developed by Hopkins [6]. Hopkins' model assumes a joint can be approximated by two parallel half-spaces separated by an asperity distribution. This model is similar to Greenwood & Williamson's model [5] where the joint was modeled as an asperity distribution in contact with a smooth flat, rigid, surface and it's later improvement by Brown and Scholtz [2] where the joint was modeled as two rough surfaces in contact. Unlike these models, Hopkins' included the interaction between contact points by allowing each of the half-spaces to deform about the asperities as well as the asperity deformation and it did not allow interpretation of the two rough surfaces like Brown and Scholtz [2]. Each asperity is modeled as a cylinder arranged on a regular lattice. The height of each cylinder is determined by the fracture generation model and is given a radius such that all cylinders initially are in contact with neighboring cylinders.

A linear system of equations can be written for this system by noting that for each asperity, the sum of the initial distance between the half-spaces, D, and the total deformation , W_i, must equal the length of the asperity, or

$$D + W_i = h_i + \Delta h_i \qquad \text{for } i \in C, \tag{3.1}$$

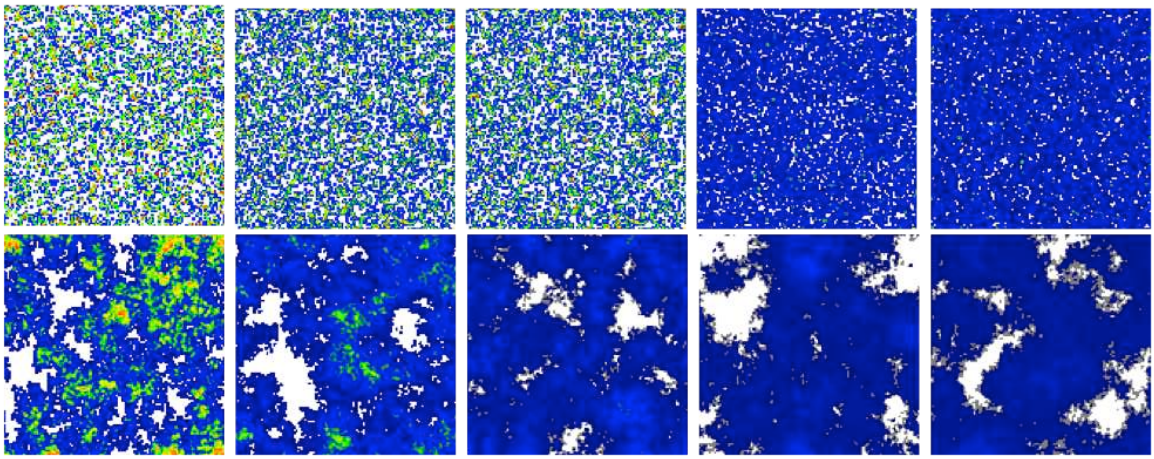

FIG. 1. *(Top row) Uncorrelated synthetic fractures generated with NPTS = 3800, 5000, 6600, 9700, 12400. (Bottom row) Correlated synthetic fractures generated with NPTS = 12, 14,16, 18, 20. The white areas are contact areas, while the color range blue to red are increasing apertures.*

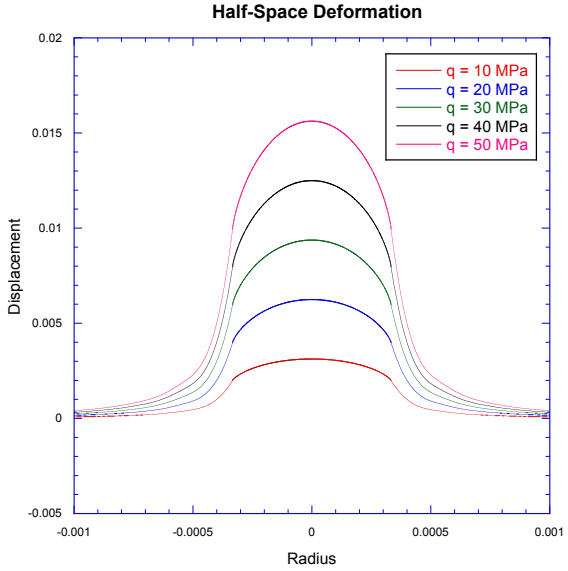

FIG. 2. *Analytic solution to the displacement of a half-space under a uniformly loaded circle of radius a = 0.003*

where C is the set of all apertures in contact, and the change in height, Δh_i is the unknown variable. The total displacement is the superposition of the self-interaction, displacement of asperity i due to the deformation of the half-space by asperity i, and the asperity-asperity interaction, displacement of asperity i due to the deformation of the half-space by asperity j. The displacement of the half-space, w_0, is found by integrating the Boussinesq's solution for a loaded circle [13] and shown in Figure 2. The solution is divided into two parts, the displacement within the loaded circle of radius a, $(r \leq a)$, and points outside the radius$(r > a)$.

$$w_0 = \begin{cases} \frac{4(1-\nu^2)qa}{\pi E} \int_0^{\pi/2} \sqrt{1-(r^2/a^2)\sin^2\theta}\, d\theta & \text{for } r \leq a \\ \frac{4(1-\nu^2)qr}{\pi E} \times \left[\int_0^{\frac{\pi}{2}} \sqrt{1-(a/r)^2\sin^2\theta}\, d\theta - \left[1-\frac{a^2}{r^2}\right] \int_0^{\frac{\pi}{2}} \frac{d\theta}{\sqrt{1-(a/r)^2\sin^2\theta}} \right] & \text{for } r > a \end{cases}$$

where,

$$\begin{aligned}
\nu &= \text{Poisson's ratio} \\
E &= \text{Young's modulus} \\
a &= \text{radius of the asperity} \\
r &= \text{the distance from the center of the asperity} \\
q &= \frac{f}{\pi a^2} = \text{stress acting on the asperity}
\end{aligned}$$

This displacement can be written in terms of the change in height Δh_i by using,

$$\Delta h_i = \frac{f_i h_i}{\pi a^2 E}. \tag{3.2}$$

To solve this system of linear equations, the conjugate gradient method was chosen [11] because it reduces the problem to a matrix-vector multiplication. The computation time for the solver was reduced by recognizing that long range interactions can be approximated accurately by Taylor expanding the half-space's displacement for large radii. By using this approximation, the matrix-vector product can be rapidly calculated by using the Fast Multipole Method, [11].

4. Flow Model. To investigate the relationship between the mechanical and hydraulic properties of fractures, a flow model is also required. The hydraulic properties of the simulated fractures considered in this study were calculated numerically using a network model similar to that of Yang et al. [16, 17], Tran [14], and Cheng et al. [3]. In this model, the aperture distribution is replaced by a connected graph starting from one inlet node and ending with one outlet node (see Figure 3).

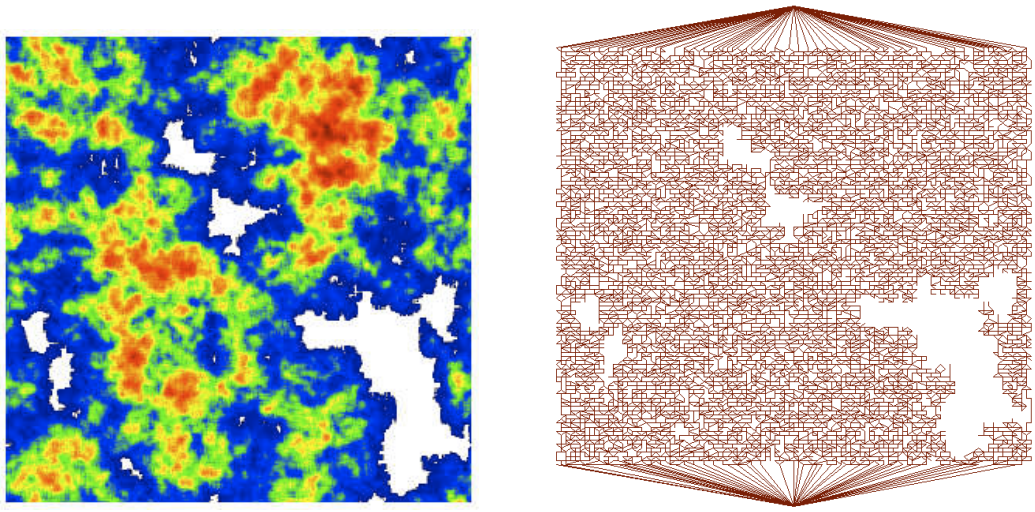

FIG. 3. *(Left) Example fracture geometry, where white is contact area and the range blue-red are increasing apertures. (Right) The resulting pipe network generated using the elliptical pipe network method.*

This differs from other models in that it is not direction blind, i.e. global flow and local flow are assumed to be in the same direction. Each row of aperture elements perpendicular to the flow is considered in turn and the large regions of non-zero apertures are brought together into a single large elliptical pipe (Figure 4). Between the rows, flow is calculated based on the analytic solution

to flow in an elliptical pipe with a hydraulic resistance based on the apertures,

$$R = \frac{4f\mu\Delta l\sqrt{K}(K+1)}{\pi a^4} \qquad \text{with,}$$
$$f = \frac{\pi a_1 b_1 + \pi a_2 b_2}{2A_{avg}} \qquad \text{and}$$
$$K = (a/h)^2 .$$

Above, a_i and b_i $i = 1, 2$, are the major and minor axis of the two ellipsis between rows, a is the average minor axis between the rows, h is half the maximum aperture of the larger ellipse, Δl is the distance between the center of the two elements, and finally A_{avg} is the average area of the two ellipses.

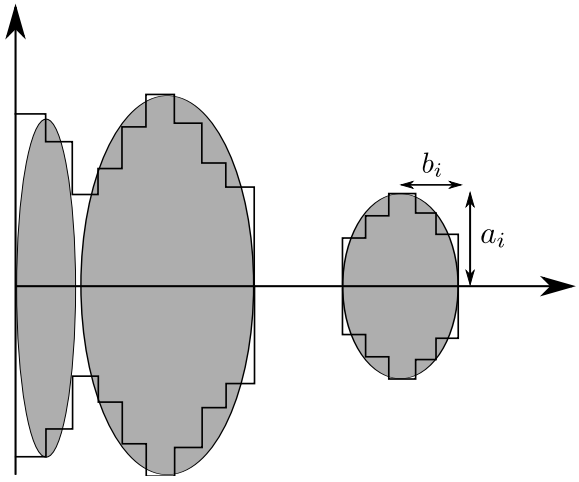

FIG. 4. *Side view of multiple apertures being converted to larger elliptical cross sections. This represents a row of a fracture geometry, perpendicular to the flow direction.*

This model is preferred over the bi-lattice grid method, used in [11], because it is computationally more efficient (run times are 4-10 times faster) and it was shown to model 2D micro-model experimental data more accurately [3].

5. Simulations. The purpose of this study is to determine the effect of the initial contact area of the fracture on both the mechanical and hydraulic properties of a single fracture. To do this, several parameter sets were chosen to generate fracture geometries to single out its effect on the mechanical and hydraulic properties. This was done by generating fractures with a constant volume, total area, and allowing the contact area fraction to vary from 0% to 40%. It should be noted that the correlated and uncorrelated generations were given constant volumes, separately, i.e. all of the uncorrelated patterns have a constant volume, V_{uncorr}, and the correlated have a volume of V_{corr}, but $V_{uncorr} \neq V_{corr}$. The parameters used are listed in Table 2.1. Because the statistical variation in the uncorrelated parameter sets was low [3], only four fractures were genereated per set, while ten were generated for the correlated.

Once the fracture geometries were generated, each was deformed under a normal load with the elastic properties of granite, i.e. a Poisson ratio of 0.25 and a Young's modulus of 60 GPa. The deformation solver was set to take between 20 to 50 steps to reach a maximum load of 80 MPa. The flow rate was computed at each step of stress. The raw numerical data are presented in Figures 5 and 6.

From the displacement-stress curves, it is observed that each of the uncorrelated and correlated (separately) fractures have the same maximum displacement. This is because they have a constant

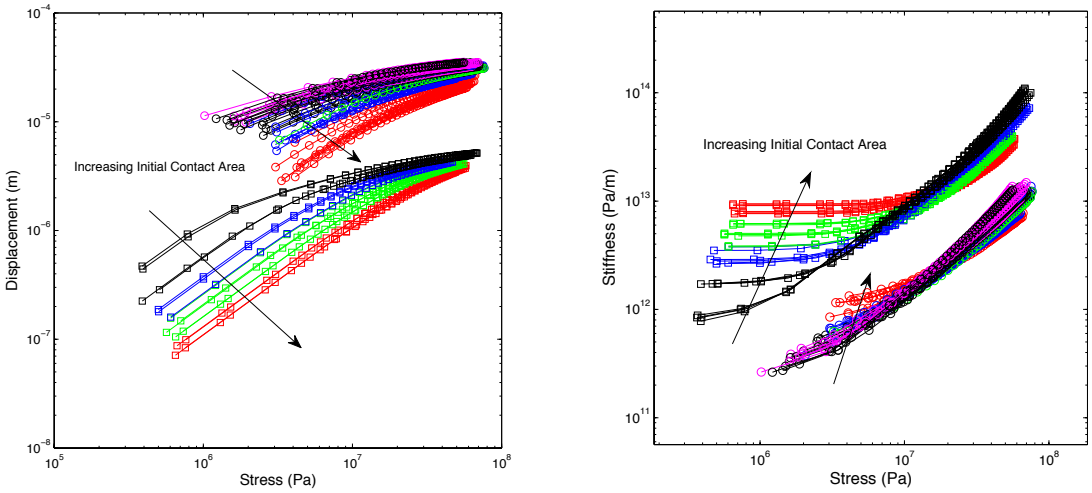

FIG. 5. *(Left) Displacement-Stress curves and (Right) Stiffness-Stress curves of the simulated fractures. Open squares are the uncorrelated (random) fractures and open circles are the correlated fractures. The color of a curve indicates its initial contact area fraction: Red = >25%, Green = 20-25%, Blue = 10-20%, Black = 5-10%, Magenta = <5%.*

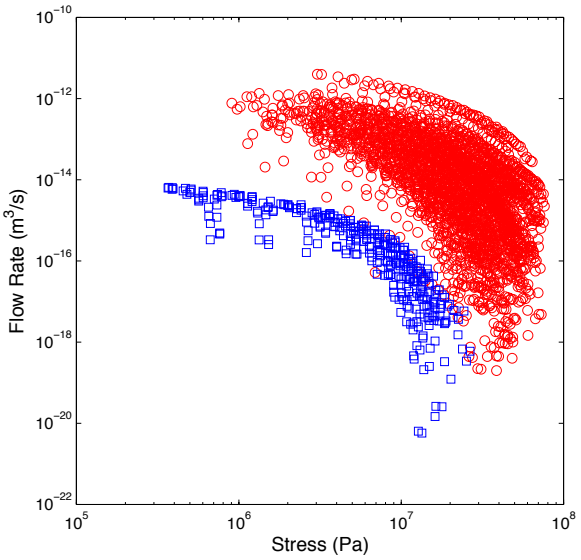

FIG. 6. *Flow-stress curves. Open squares are the uncorrelated (random) fractures and open circles are the correlated fractures.*

volume. However, it can also be seen that the curves diverge at low stresses. The colors of the curves signify their corresponding initial contact fraction. Red curves signify that the generated fracture has a initial contact fraction of >25%, green means that it was between 20-25%, blue curves have between 10-20%, black curves have between 5-10%, and finally, magenta curves have less than 5% initial contact area fraction. From this, it is observed that the difference between the curves is caused by the difference in their initial contact area. As expected, the dispersion in the correlated patterns is much larger than that of the uncorrelated, but the same trend can be seen. The stiffness-stress curves exhibit a similar divergence as the displacement stress curves. However this is expected because fracture stiffness is just the inverse slope of the tangent line on the displacement-stress curves.

As stated before, the flow rate of each fracture was calculated for each stress step. Unfortunately, the flow rate is dependent on more than only the initial contact area. Fluid flow through a fracture depends on the void areas, rather than contact, and is fundamentally defined by its continuum percolation properties. For these reasons, the flow-stress curves, Figure 6, can not be normalized as simply as the mechanical attributes, as will be shown in section 6. However the flow rate can be bounded, for both the correlated and uncorrelated together, by utilizing the initial void area fraction.

6. Results and Disscussion. The different fracture geometry realizations yielded disparate displacmenet-stress (Fig 5), stiffness-stress, and flow-stress (Fig 6) relationship. Using these numerical results, we investigated whether or not these results could be collapsed to a single functional relationships. Figure 7 shows the normalization found for the displacement and stiffness as a function of stress for the simulated fracture geometries. In Figure 7, the displacement is normalized by the initial volume and the stress is normalized by the initial contact area fraction. This normalization of the displacement effectively suppresses the maximum displacement of the uncorrelated and correlated curves to the same value leaving only the "knees" of the curves unnormalized. Normalizing the stress by the initial contact area fraction suppresses the starting point of each curve to the same value. To complete the stiffness normalization, the stress axis is divided by the initial contact area fraction for the same reasons as the displacement curves. The stiffness is then divided by the initial contact fraction as well to keep the unit area consistent.

These normalizations imply that the initial contact area fraction is a fundamental quantity of the mechanical properties of fractures. In other words performing a finite-size scaling measurement without this normalization would be impossible because there would be two disparate effects occurring, (1) the dispersion due to the initial contact area fraction and (2) the scaling effect. Without the dispersion due to the initial contact area fraction, future studies can study the scaling effects of the mechanical properties of fractures, i.e. the change of fracture areal size.

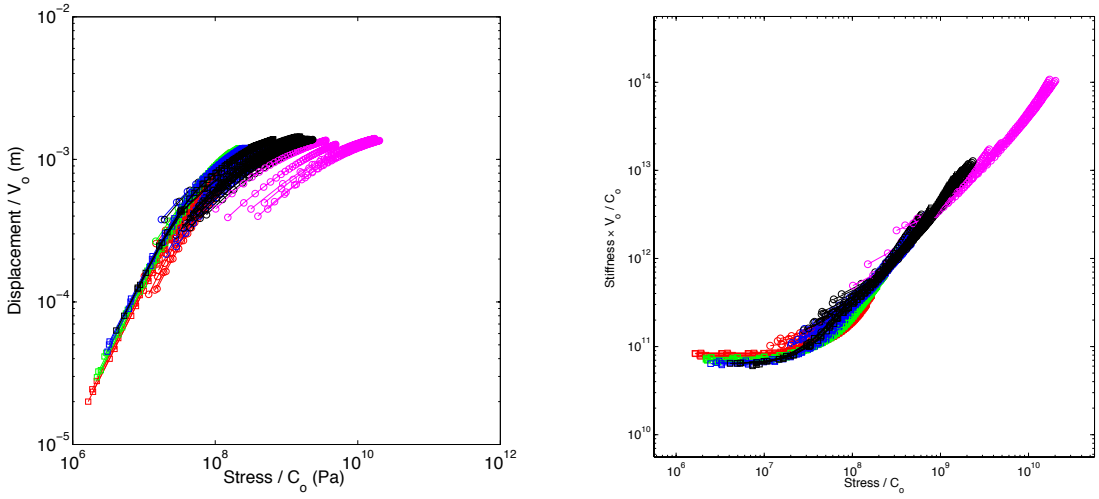

FIG. 7. *Normalized displacement-Stress curves (left) and stiffness-stress curves (right) of the simulated fractures. Open squares are the uncorrelated (random) fractures and open circles are the correlated fractures. The color of a curve indicates its initial contact area fraction: Red = >25%, Green = 20-25%, Blue = 10-20%, Black = 5-10%, Magenta = <5%.*

The displacement as a function of the contact area fraction is shown on Figure 8. In this case, each of the generation parameter sets are averaged into a single curve. To normalize this family of curves, the initial contact area fraction is subtracted from the contact area fraction at each stress. Then the displacement is multiplied by the contact area's correlation length raised to the exponet $-1/1.33$ and divided by the initial volume. The correlation length was determined by the decay

constant of the autocorrelation of the contact and the exponent is the critical exponent found in 2D percolation theory. This normalization does not remove the difference between the correlated and uncorrelated fractures, yet it does reduce the family of curves to two functional relationships. Whether the correlated and uncorrelated displacement-contact area fraction curves can be collapsed to a single curved is not known at this time. This implies that within each subfamily (uncorrelated and correlated), the initial contact area fraction and the correlation length are fundamental quantities required to study the scaling of the displacement as a function of contact area fraction. Within the subfamilies, a finite-size scaling analysis can now be preformed to understand the critical phenomena at threshold ($C_f = 0$). It is imperative that we understand this function in order to determine if a relationship between the mechanical and the hydraulic properties exists that depends on the criticality of the flow properties that are dominated by the void area fraction.

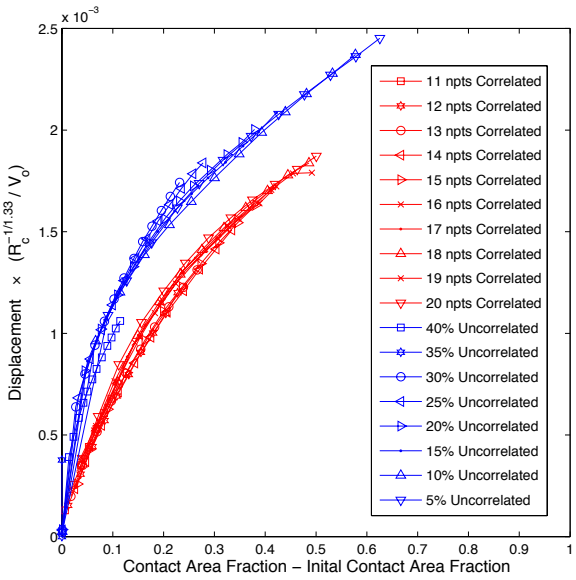

FIG. 8. *Normalized displacement for each set of simulation parameters, after averaging, as a function of contact area.*

As mentioned in section 5, a complete normalization of the hydraulic properties is not presented here, rather a normalization that bounds the potential flow curves as a function of stress. To bound the flow rate, scaling parameters from standard percolation theory are used, such as, $(A - A_c)^{-\nu}$, where A_c is the critical area fraction – $A_c = 0.6$ for uncorrelated patterns and $A_c = 0.5$ for correlated ones. As seen in Figure 9, the flow is scaled by dividing by the initial flow rate, and multiplying by the ratio of $(A_f - A_c)$ to $(A_o - A_c)$ raised to the -1.2 power. The stress is scaled by subtracting the initial stress, multiplying by the ratio of the total displacement to the initial mean aperture, and dividing by the initial volume to the 1/3 power. The normalized stress has the same units as fracture specific stiffness, and thus Figure 9 can be viewed as a flow-stiffness normalization as well. Figure 9 also shows two signatures expected from Percolation Theory. The curves are tightly bounded at low stresses because void area fraction is very high, i.e. this regime can be considered as an effective medium. As the stress is increased, the void area fraction grows and the percolation properties approach the critical threshold. As this occurs, the length scales diverge and the flow properties disperse as well.

7. Conclusion. In this paper, we attempt to remedy the issue of uniqueness for a fracture at a given void/contact area fraction. This was done by normalizing the mechanical properties of joint deformation, displacement and stiffness, onto a single curve. By doing this, we can correctly identify the displacement or stiffness of any fracture with the knowledge of its initial contact area

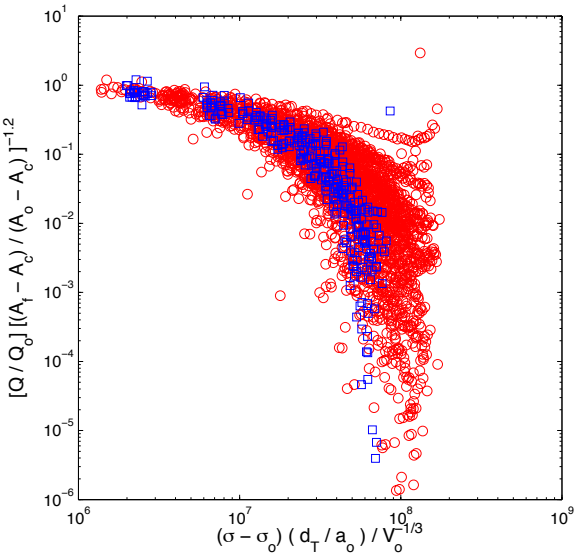

FIG. 9. *Normalized flow-stress curves.* □ *are the uncorrelated (random) fractures and* ◯ *are the correlated fractures, where on the y-axis* Q *is the flow rate,* A_f *is the void area fraction,* A_c *is the critical void area fraction, and*A_o *is the initial void area fraction. The x-axis consists of the stress,* σ*, the initial stress,* σ_o*, the total displacement,* d_T*, the initial mean aperture height,* a_o*, and the initial volume,* V_o*.*

fraction, however, at the low initial contact area fraction limit the correlated fracture planes exhibit dispersion. We also presented a normalization for the average behavior of the displacement as a function contact area fraction. In this case, the correlated and uncorrelated sets could be normalized individually only, which suggests that in order to consider the mechanical properties as a function of contact area fraction requires another length scale. Lastly, we present a normalization that bounds the flow-stress curves.

8. Acknowledgments. The authors wish to acknowledge Joe Morris for his assistance with code development. The authors wish to acknowledge support of this work by the Geosciences Research Program, Office of Basic Energy Sciences US Department of Energy (DEFG02-97ER14785 08), the GeoMathematical Imaging Group at Purdue University and from the Computer Research Institute At Purdue University.

REFERENCES

[1] FM Borodich and DA Onishchenko. Similarity and fractality in the modelling of roughness by a multilevel profile with hierarchical structure. *International Journal of Solids and Structures*, 36(17):2585–2612, 1999.

[2] SR Brown and CH Scholz. Closure of random elastic surfaces in contact. *Journal Of Geophysical Research-Solid Earth And Planets*, 90(NB7):5531–5545, 1985.

[3] J.T. Cheng, J.P. Morris, J. Tran, A. Lumsbaine, N.J. Giordano, D.D. Nolte, and L.J. Pyrak-Nolte. Single-phase flow in a rock fracture: micro-model experiments and network flow simulation. *International Journal of Rock Mechanics and Mining Sciences*, 41:687–693, 2004.

[4] PWJ Glover, K Matsuki, and K Hayashi. Synthetic rough fractures in rock. *Journal of Geophysics Research - Solid Earth*, 103:9609–9620, 1998.

[5] J. A. Greenwood and J. B. P. Williamson. Contact of nominally flat surfaces. *Proceedings of the Royal Society of London. Series A, Mathematical and Physical Sciences*, 295(1442):300–319, 1966.

[6] D.L. Hopkins. *The Effect of Surface Roughness on Joint Stiffness, Aperture, and Acustic Wave Propagation.* PhD thesis, 1990.

[7] DD Nolte and LJ Pyrak-Nolte. Stratified continuum percolation - scaling geoemetry of hierarchical cascades. *Physical Review A*, 44(10):6320–6333, 1991.

[8] DD Nolte and LJ Pyrak-Nolte. Coexisting two-phase flow in correlated two-dimensional percolation. *Physical Review E*, 56(5, Part A):5009–5012, 1997.

[9] DD Nolte, LJ Pyrak-Nolte, and NGW Cook. The fractal geometry of flow paths in natural fractures in rock and the approach to percolation. *Pure and Applied Geophysics*, 131(1-2):111–138, 1989.
[10] H. Peitgen and D. Saupe. *The science of fractal images*. Springer, 1988.
[11] L.J. Pyrak-Nolte and J.P. Morris. Single fractures under normal stress: The relation between fracture stiffness and fluid flow. *International Journal of Rock Mechanics and Mining Sciences*, 37:245–262, 2000.
[12] Dietrich Stauffer and Amnon Aharony. *Introduction to Percolation Theory*. CRC Press, 1985.
[13] S.P. Timoshenko and J.N. Goodier. *Theory of elasticity 3rd ed.* McGraw-Hill, 1970.
[14] J.J. Tran. *Efficient simulation of multiphase flow in three-dimensional fracture netowrks*. PhD thesis, 1998.
[15] R. Walsh, C. McDermott, and O. Kolditz. Numerical modeling of stress-permeability coupling in rough fractures. *Hydrogeology Journal*, 16:613–627, 2008.
[16] G. Yang, N.G.W. Cook, and L.R. Myer. Network modelling of flow in natural fractures as a guide for efficient utilization of natural resources. *Proceedings of 30th US Symposium on Rock Mechanics*, pages 57–64, 1989.
[17] G. Yang, L.R. Myer, S.R. Brown, and N.G.W. Cook. Microscopic analysis of macroscopic transport-properties of single natural fractures using graph-theory algorithms. *Geophys Res Lett*, 1995.